Intramolecular electron transfer in multi-redox systems based on cyclic [3]spirobifluorenylene compound

Tomoya Imai,[a] Daisuke Sakamaki,[b] Shinobu Aoyagi,[a] and Toru Amaya*[a]

[a] *Department of Information and Basic Science, Graduate School of Science, Nagoya City University, 1 Yamanohata, Mizuho-cho, Mizuho-ku, Nagoya, Aichi 467-8501, Japan.*

[b] *Department of Chemistry, Graduate School of Science, Osaka Metropolitan University, Naka-ku, Sakai, Osaka 599-8531, Japan.*

E-mail: amaya@nsc.nagoya-cu.ac.jp

Abstract

Cyclic [3]spirobifluorenylene with bulky alkyl groups at the ends (**1**) was designed and synthesized to investigate the electron transfer phenomena in a π-conjugated system including orthogonal π-conjugated chains. The three bifluorenyl units in **1** are conjugated to each other via spiro-conjugation, resulting in the splitting of the HOMO levels to a small extent. Therefore, the SOMO–HOMO gap of the radical cation species is small, which is considered to allow the facile intramolecular electron transfer. The electronic properties of **1** and its partial structures were characterized by absorption and fluorescence measurements and electrochemical analysis. From the electrochemical oxidation, the interchain Coulombic repulsion was observed. In the TD-DFT calculations for the radical cation species of **1**, the geometry-featured interchain electronic transitions were visualized by NTO calculations. The radical cation species of **1** generated by chemical oxidation with $SbCl_5$ exhibited a broadened and lower-energy shifted NIR absorption band compared to those of its partial structures. Considering the results of the TD-DFT calculations, the NIR band of the radical cation of **1** was attributed to the intramolecular electron transfer processes among the bifluorenyl units in the macrocycle. ESR experiments also indicated the delocalization of a spin of $\mathbf{1}^{\cdot+}$ in the whole molecule via hole hopping. This work demonstrates the usefulness of spiro-conjugation as a bridging unit in molecular wires to facilitate smooth electron transfer.

Introduction

The transfer of charge carriers, such as electrons and holes, within molecules is one of the key fundamental processes in organic electronics, including molecular electronics.[1] Organic compounds with multiple redox-active units can generate mixed-valence states whose redox-active units have different valences (redox states) (Figure 1a) and have been widely studied as models of molecular wires.[2] In particular, even in the mixed-valence molecules with apparently non-conjugated redox units, electron transfer through spatial orbital interactions and electron hopping are possible, which are important for understanding macroscopic electronic transport.[3] Spiro-compounds are a class of compounds with small spatial electronic conjugation.[4] Spirobifluorene, which has an orthogonal

arrangement of biphenyl units sharing a spirocarbon, is known as a typical spiro-compound of π-conjugated molecules, which can be great potential for material applications.[5] In this molecule, the orbital interactions by spiro-conjugation[6] cause the splitting of HOMOs of each fluorene unit. Although some π-conjugated spiro-compounds, such as 2,2',7,7'-tetrakis[N,N-di(4-methoxyphenyl)amino]-9,9'-spirobifluorene (spiro-OMeTAD), are widely used as hole-transport materials of OLED and perovskite solar cells, [7] studies on intramolecular electron transfer in the π-conjugated systems including orthogonal π-conjugated planes have been very limited so far (Figure 1b).[8,9] Nakamura et al. generated radical cation species in spiro-conjugated carbon-bridged *p*-phenylenevinylenes, showing efficient charge delocalization desirable for hole transport materials.[9e] Rathore et al. investigated the Coulombic interaction between two orthogonal chromophores using radical cation species of spirobifluorene compounds terminated with cyclic alkyl or MeO groups, but molecules with more than three fluorene units were not investigated in the study.[10]

Recently, we have reported the synthesis of shape-persistent macrocyclic compounds with a chiral spirobifluorene as a building block.[11] Among them, cyclic [*n*]spirobifluorenylenes (Figure 1c) have an interesting structural feature in that the bifluorenyl units are linked by a spiro-linkage to form a macrocycle.[11b] The spiro-conjugation in cyclic [*n*]spirobifluorenylenes showed a characteristic even-odd effect depending on the number of bifluorenyl chromophores. The small orbital splitting of the frontier MOs due to the small electronic coupling by spiro-conjugation has been estimated by theoretical studies based on density functional theory (DFT) calculations (Figure 1c). In this context, we conceived that the facile intramolecular electron transfer among bifluorenyl units can occur in radical cationic species due to the small energy gap between SOMO and HOMO, whereas there exist through-space overlaps of molecular orbitals of bifluorenyl units around the spirocarbons. (Figure 1d). If the radical cation species of cyclic [*n*]spirobifluorenylenes is generated by one-electron oxidation, the energy barrier for interchain charge transfer would be very low due to the small HOMO–SOMO gap. In general, the splitting of the HOMO could be reduced if two or multiple identical redox units are far apart from each other, but efficient electron transfer cannot be expected in such a situation. On the other hand, spiro-conjugation not only makes the energy difference between redox units extremely small but also affords electron transfer via spatial overlap between the redox units. Such electron transfer via spiro-conjugation in cyclic systems has never been investigated in the past. In a previous study, we performed electrochemical oxidization of the cyclic [*n*]spirobifluorenylenes (n = 3–5) and found that the compounds exhibited completely irreversible voltammograms, indicating the instability of the cationic species.[11b] The decomposition of the oxidized species was thought to be caused by the subsequent side reactions at the unsubstituted fluorene termini. To avoid the side reactions, in this study, we designed and synthesized a cyclic [3]spirobifluorenylene with bulky alkyl groups at the ends of each spirobifluorenylene unit (**1**) (Figure 1d). This compound is expected to have increased stability in the cationic states enough to investigate the redox behavior and the properties of the cationic states.

Here, we report the synthesis of **1** and its intramolecular electron transfer behavior in the radical cation species. This study will provide examples of electron transfer behavior in multi-redox systems connected through spiro-conjugation in a cyclic manner, which have not been reported so far, and is expected to afford new design guidelines for next-generation charge-transport materials.

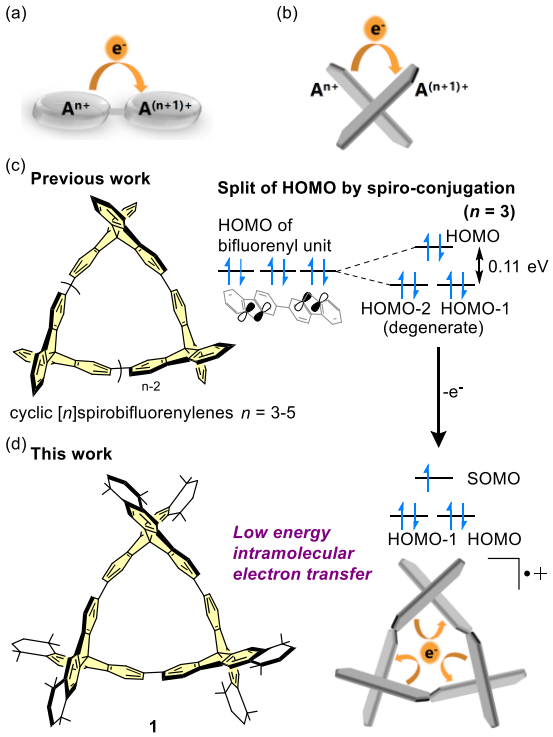

Figure 1. (a) Schematic illustration of electron transfer in a mixed valence organic compound and (b) between orthogonal π-conjugated planes. (c) Previous work on cyclic [*n*]spirobifluorenylenes and spiro-conjugation in the case of $n = 3$.[11b] (d) This work on intramolecular electron transfer in the radical cation of **1**.

Results and discussion

Scheme 1 shows the synthetic scheme of the cycloalkylated compounds **1**, and its model compounds **2** and **3** which are the partial structures of the macrocycle **1**. Compound **1** and model compounds **2** and **3** were synthesized by double Friedel-Crafts alkylation using 2,5-dichloro-2,5-dimethylhexane. The purification of all compounds was carried out by the preparative recycling HPLC with tandemly arranged two GPC columns for the complete purification in order to use the subsequent measurements. All the products were confirmed by ^{1}H and ^{13}C NMR spectra and MALDI-TOF-MS analyses. Single crystals of (*P*,*P*,*P*)-**1** were obtained from a toluene/MeOH solution. X-ray crystallographic analysis showed two crystallographically independent molecules in the unit cell (Figure 2 and Figure S1), but there were no characteristic differences between them. The macrocycle **1** had a triangle-shaped structure, slightly deviated from a complete D_3-symmetric structure in the

monoclinic crystal. The averaged dihedral angle between the spirobifluorene units, distortion around the spirocarbon, and the distance between the spirocarbons of (*P*,*P*,*P*)-**1** were 46.1°, 87.8°, and 8.6 Å (Figure. S1 for unit cell of the crystal structure).

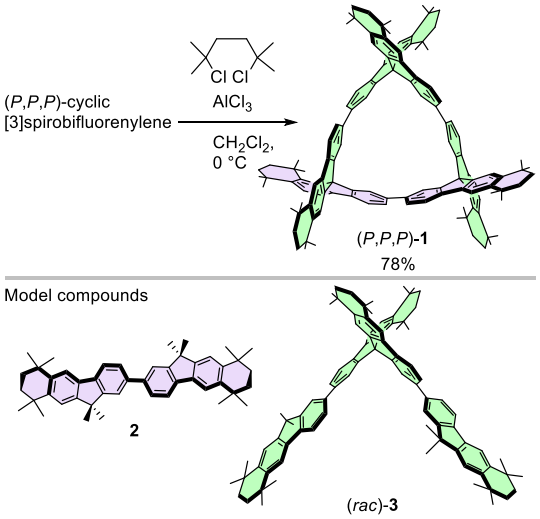

Scheme 1. Synthesis of **1**, and its model compounds **2** and **3**.

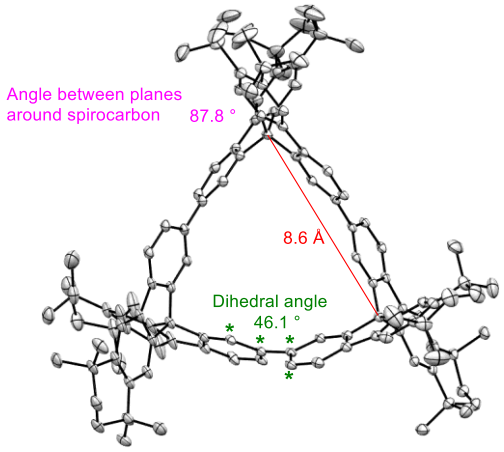

Figure 2. ORTEP drawing of (*P*,*P*,*P*)-**1** with thermal ellipsoids set at the 30% probability level. One of the two independent molecules is shown. Hydrogen atoms, disordered structures, and solvent toluene molecules are omitted for the sake of clarity. The values of the dihedral angle, distortion around the spirocarbon, and the distance between the spirocarbons are averaged.

The UV-Vis absorption and fluorescence spectra of **1**, **2**, and **3** are shown in Figure 3a and 3b. The maximum absorptions for **1**, **2**, and **3** were observed at 334, 335, and 338 nm, respectively, as the lowest energy absorption bands. Compared to the unsubstituted macrocycles, the cycloalkylated compound **1** showed a slight blue shift in the maximum absorption due to the electron-donating effect of the alkyl groups. The red-shift of **3** toward **2** indicates spiro-conjugation. In the case of **1**, the effects

of spiro-conjugation and twisting between fluorenes (Figure S3) due to structural constraint may have been cancelled out, giving a spectrum very close to that of **2**. The fluorescence spectrum of **1** showed peaks at 372 and 387 nm, exhibiting violet-coloured emission (Figure 3b) with high quantum yields (80%). The chiroptical properties of **1** were investigated based on circular dichroism (CD) spectroscopy (Figure S2). The enantiomers exhibited mirror-imaged CD spectra with the dissymmetry factor ($|g_{abs}|$) of 6.8×10^{-3} at 346 nm.

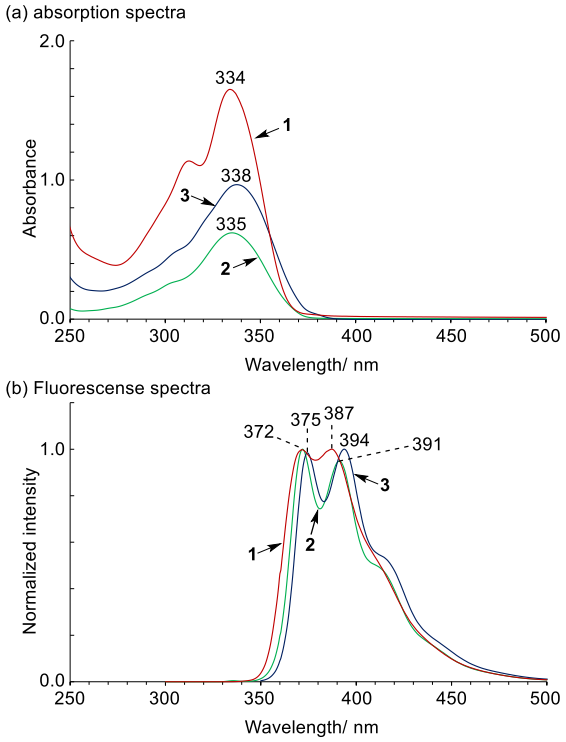

Figure 3. (a) Absorption and (b) fluorescence spectra for **1**, **2**, and **3** in CH_2Cl_2 using 1.0 x 10^{-2} m cuvette (1.0 x 10^{-5} M). Excitation wavelength for **1**, **2**, and **3** are 341, 335, and 335 nm, respectively.

The electrochemical multi-electron oxidation behavior of the macrocycle **1** and the model compounds **2** and **3** was investigated by cyclic voltammetry (CV) and square wave voltammetry (SWV) in CH_2Cl_2 solutions containing NBu_4BF_4 at room temperature. Figure 4 shows the voltammograms of **1**, **2**, and **3**. The simulated SWVs[12] are also shown in Figure 4. Before discussing the multi-electron oxidation behavior of **1**, acyclic model compounds **2** and **3** were first examined. Model bifluoreneyl compound **2** exhibited two successive reversible one-electron oxidation processes in the CV (Figure 4a). The oxidation potentials of **2** determined by the SWV are 0.77 and 1.04 V vs Fc/Fc^+, respectively. In the case of SWV for model compound **3**, two sharp peaks (0.79 and 0.93 V) attributable to successive one-electron oxidation and one broad peak (1.28 V) attributable to nearly simultaneous two-electron oxidation were observed in the positive scan (Figure 4b). The simulation

reproduced the experimental voltammograms. The first oxidation potential of **3** was almost the same as that of **2**, which clearly shows the small electronic coupling around spirocarbon. However, the splitting of the initial two electron oxidation waves of **3** clearly indicates the existence of Coulombic interactions between the two orthogonal bifluorenyl units. This result is consistent with the previous report of Rathore and co-workers.[10] With the information in hand, the macrocycle **1** was then examined. The protection of **1** was clearly effective in preventing side reactions in the cationic states, and the almost reversible waves were observed in the CVs of **1**, in contrast to those of the unsubstituted ones. Three peaks (0.79, 0.93, and 1.04 V) attributable to one-electron oxidation from each bifluorenyl unit and one broad peak (1.28 V) attributable to nearly simultaneous three-electron oxidation were observed in the positive scan of the SWV (Figure 4c). The SWV was well reproduced by the simulation. The observed stepwise three one-electron oxidation processes can be accounted for by Coulombic interactions among the three bifluorenyl units.

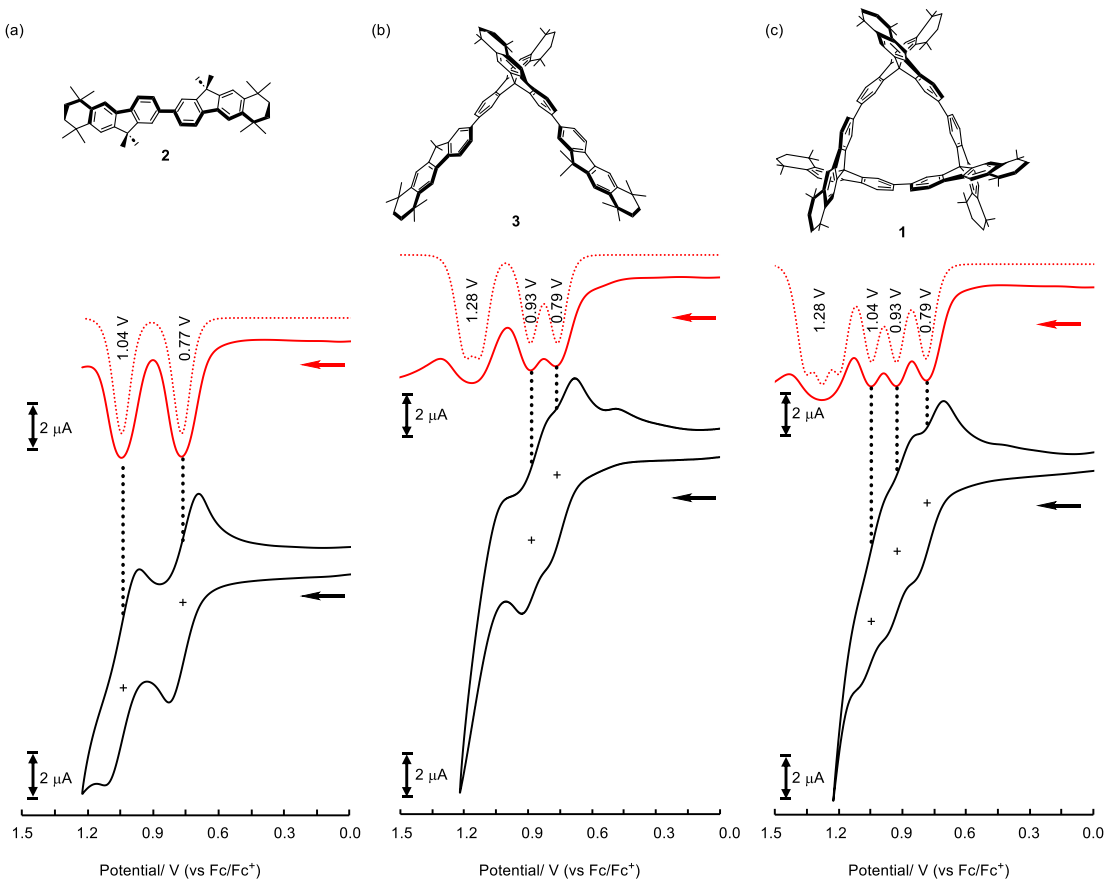

Figure 4 CVs (black line), SWVs (red line), and simulations (red dotted line) for SWVs of (a) **2**, (b) **3**, and (c) **1**. Concentration: 1.0×10^{-3} M in CH_2Cl_2 containing 5.0×10^{-2} M NBu_4BF_4 as a supporting electrolyte. The values were obtained from SWVs, which were recorded with 100 mV/s of scan rate at a platinum electrode under Ar.

The structure and electronic properties of **1** and its model compounds **2** and **3** were estimated using DFT calculations at the B3LYP-D3/6-31G(d,p) level of theory. The structural optimization of **1** was carried out with D_3 point group symmetry. The distance between the spirocarbon units, distortion around the spirocarbon, dihedral angle between the spirobifluorene units, and frontier molecular orbital energies are summarized in Figure 5, S3, S4, and Table S1. The energies of both HOMO and LUMO of **1**, particularly the HOMO, are higher than those of the corresponding unsubstituted 3-mer due to the electron-donating cyclic alkyl groups. As described briefly in the introduction, cyclic [*n*]spirobifluorenylenes have characteristic cyclic spiro-conjugation consisting of multiple bifluoreneyl chromophores linked by sharing spirocarbons. Figure 5 shows the calculated energies and drawings of the HOMO to HOMO−2 for **1**, while the corresponding information for the splitting of the LUMOs are shown in Table S1 and Figure S4. The three occupied and three unoccupied frontier MOs of **1** split into 1:2 and 2:1, respectively. The HOMO was 0.10 eV above the doubly degenerate HOMO−1 and HOMO−2, and the LUMO was 0.05 eV below the doubly degenerate LUMO+1 and LUMO+2. The obtained splitting patterns and such small energy splitting are similar to the corresponding unsubstituted macrocycle.[11b] Next, we performed the structural optimization and TD-DFT calculations for the radical cation states of **1**–**3**. For the calculations of $\mathbf{1}^{\cdot+}$–$\mathbf{3}^{\cdot+}$, we used the calculation conditions reported by Kaupp et al. to provide reliable results for simulating organic MV systems (BLYP + 35% Hartree-Fock (HF)-like exchange and SVP basis sets combined with a continuum solvent model)[13]. The calculated energies and optimized structures of $\mathbf{1}^{\cdot+}$, $\mathbf{2}^{\cdot+}$, and $\mathbf{3}^{\cdot+}$ are shown in Table S2 and Figure S5. The dihedral angles between the fluorene units in model compound $\mathbf{2}^{\cdot+}$ decreased, and the fluorene units were planarized compared with their neutral states (38.0° and 17.4° for **2** and $\mathbf{2}^{\cdot+}$, respectively). Concerning $\mathbf{2}^{\cdot+}$, the crystal structure was obtained (Figure S8), and the planarized structure was exhibited (average 17.5°). The symmetry of the crystal structure also reveals that the spin is not localized in one fluorenyl unit but rather delocalized throughout the bifluorenyl unit. In model compound $\mathbf{3}^{\cdot+}$, the optimized structure was unsymmetrical. That is, one bifluorenyl unit was flattened while the other was twisted. Spin density calculations clearly showed that the spin was localized in one of the chains (Figure S7). Similarly, in the structure of cyclic compound $\mathbf{1}^{\cdot+}$, one bifluorenyl unit was flattened, and visualization of the spin density showed that the spin was indeed localized there (Figure S7). The HOMO–SOMO (β-LUMO) energy gap of $\mathbf{1}^{\cdot+}$ was 1.15 eV (Table S2), which is slightly larger than the gap between the HOMO and HOMO−1 in neutral compound **1**. The results of the TD-DFT calculations and the Natural Transition Orbital (NTO) of $\mathbf{1}^{\cdot+}$, $\mathbf{2}^{\cdot+}$, and $\mathbf{3}^{\cdot+}$ are shown in Figure 6. For the model compound $\mathbf{2}^{\cdot+}$, the absorption peak in the NIR region was estimated at 1224 nm, which was assigned to the HOMO–SOMO (β-HOMO–β-LUMO) transition (Figure 6a). For model compound $\mathbf{3}^{\cdot+}$, the absorption peaks at 1285 and 2266 nm were estimated; the results of NTO analysis suggest that the former is a transition between identical

bifluorenyl chains, as in model compound $\mathbf{2}^{\cdot+}$, whereas the latter is a transition between different bifluorenyl chains. The TD-DFT simulation for $\mathbf{1}^{\cdot+}$ is similar to $\mathbf{3}^{\cdot+}$. The transition 5 for 2346 nm can be accounted for by interchain charge transfer transitions, as shown in NTO analysis.

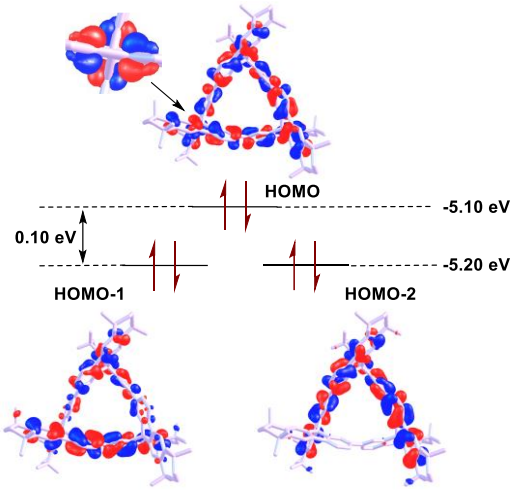

Figure 5 Calculated energies and drawings of HOMO to HOMO−2 for **1** [B3LYP-D3/6-31G(d,p)] (contour value is 0.025).

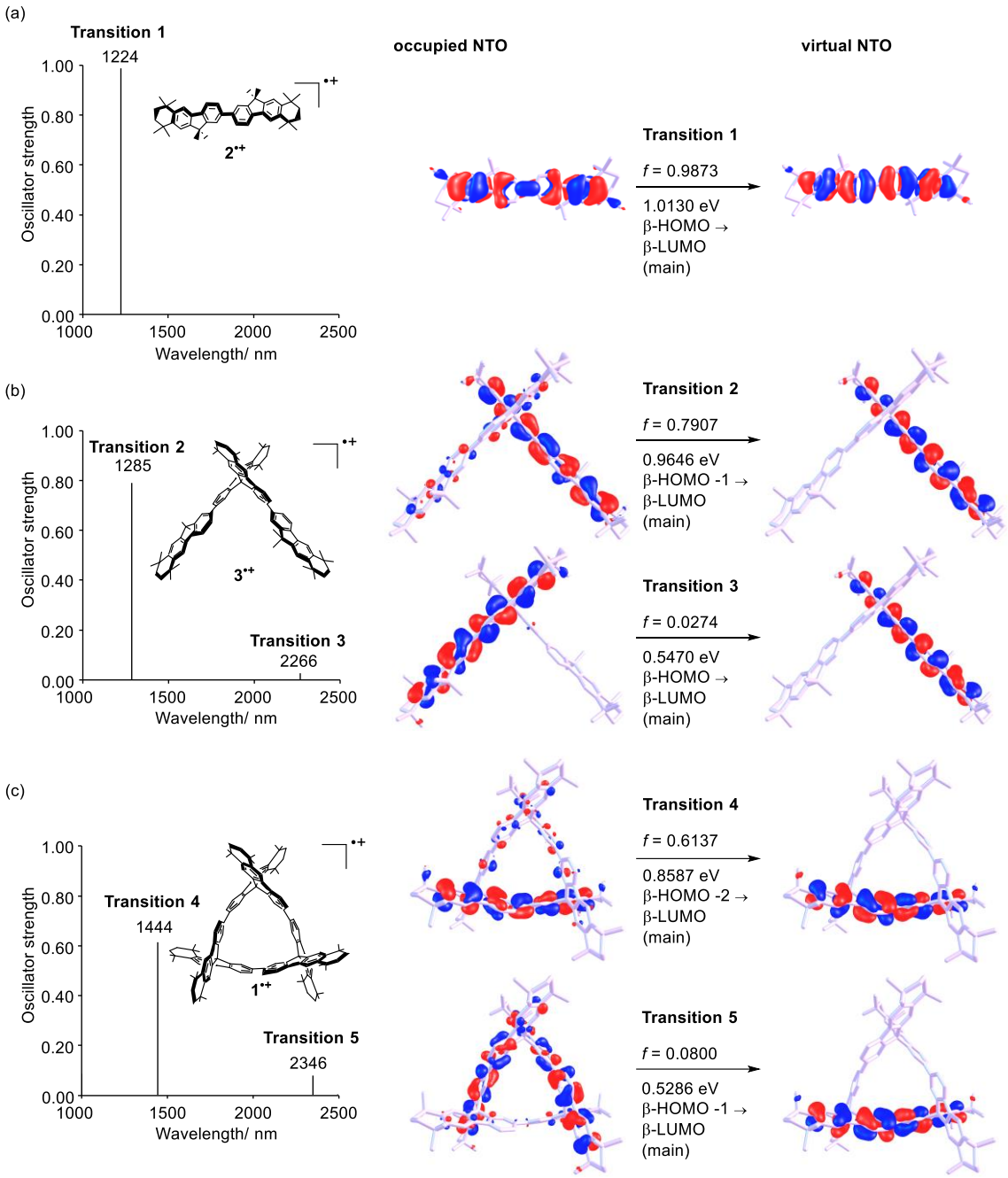

Figure 6 TD-DFT calculation and NTO for (a) $\mathbf{2}^{\bullet+}$, (b) $\mathbf{3}^{\bullet+}$, and (c) $\mathbf{1}^{\bullet+}$ based on UBLYP35/SVP+CPCM(CH_2Cl_2) level of theory for both structural optimization and TD-DFT calculation.

The electron transfer behavior in the radical cation species of **1**–**3** was investigated by monitoring the changes in the NIR region of the absorption spectra. The sequential addition of $SbCl_5$ generated the radical cation species, and the absorption spectra were recorded each time. Figure 7a shows the results of experiments using high concentration solutions of **1**–**3** (100 μM) to generate

mono-radical cation species selectively. With the addition of $SbCl_5$ up to 1.5 equivalents (1 molar equivalent based on one-electron oxidation[14]), new peaks in the NIR region appeared. The maximum wavelengths (λ_{max}) were 1400, 1440, and 1560 nm for model compounds $\mathbf{2}^{\cdot+}$, $\mathbf{3}^{\cdot+}$, and macrocycle $\mathbf{1}^{\cdot+}$, respectively, which can be assigned to the transitions for the charge resonance band. The shapes of the peaks were broadened in the order of $\mathbf{2}^{\cdot+}$, $\mathbf{3}^{\cdot+}$, and $\mathbf{1}^{\cdot+}$. In particular, the low-energy tail of the NIR band of $\mathbf{3}^{\cdot+}$ and $\mathbf{1}^{\cdot+}$ exceeded 2000 nm. The observed low-energy tails of $\mathbf{3}^{\cdot+}$ and $\mathbf{1}^{\cdot+}$ can be assigned to the intervalence charge transfer (IVCT) band among the different bifluorenyl chains, which were expected by the TD-DFT calculations to be the lowest-energy transitions (Figure 6b and 6c). As described below, the present oxidation reaction with $SbCl_5$ requires the addition of a large excess of $SbCl_5$ for the subsequent multi-electron oxidation reaction (Figure 7b). The redox equilibrium position after the addition of 1.5 equivalents of $SbCl_5$ is considered to be far to the left. Therefore, the observed IVCT bands are likely to be derived from mono-radical cation species. On the other hand, the intermolecular interactions of the radical cation species with neutral species would be suppressed due to the bulky alkyl substituents.

To follow the spectral changes upon further oxidation, similar experiments using lower concentration solutions (10 μM) were performed (Figure 7b). In the case of model compound **2**, the absorption peak around 1400 nm increased first, indicating the formation of radical cation species $\mathbf{2}^{\cdot+}$. After the addition of more than 250 equivalents of $SbCl_5$, the peak around 1400 nm started to decrease, and a new peak around 850 nm increased. Finally, the absorption around 1400 nm disappeared and changed to the peak around 850 nm after adding 1000 equivalents of $SbCl_5$. This suggests the formation of dication species $\mathbf{2}^{2+}$. For **3**, the peak around 1440 nm attributable to $\mathbf{3}^{\cdot+}$ shifted to 1370 nm by further oxidation, accompanying the peak broadening. Upon further addition of $SbCl_5$, the peak around 1370 nm started to decrease, and a new peak at 860 nm appeared. Judging from the results of **2** and the electrochemical measurements of **3**, the absorption at 1370 nm could be attributed to $\mathbf{3}^{2+}$. Concerning the absorption at 860 nm, it could be attributed to the dication species localized on a bifluorenyl unit, like $\mathbf{2}^{2+}$. The oxidation potentials of the third and fourth electrons are close in the SWV of **3**, so the highly oxidized species $\mathbf{3}^{3+}$ and $\mathbf{3}^{4+}$ are likely to be mixed in equilibrium in the system. The complete oxidation to $\mathbf{3}^{4+}$ cannot be conducted. In the case of macrocycle **1**, after the increase of the peak around 1560 nm attributable to $\mathbf{1}^{\cdot+}$, this peak shifted to around 1370 nm similar to the case of **3**. Upon further oxidation, the peak around 1370 nm decreased, and a new peak around 1040 nm increased. Judging from the results of the model compounds and the electrochemical measurements of **1**, the absorption at 1370 nm could be attributed to $\mathbf{1}^{3+}$ and 1040 nm to the higher oxidized states of **1**. The absorption peak of the higher oxidized species of **1** bearing two positive charges in each bifluorenyl unit (1040 nm) was red-shifted compared to those of $\mathbf{2}^{2+}$ and $\mathbf{3}^{4+}$ (and/or $\mathbf{3}^{3+}$) (850 and 860 nm). This can be accounted for by the small planarity due to the structural regulation of the macrocyclic system. The complete oxidation of **1** could not be accomplished with this oxidant

due to the strong Coulombic repulsion in the macrocycle.

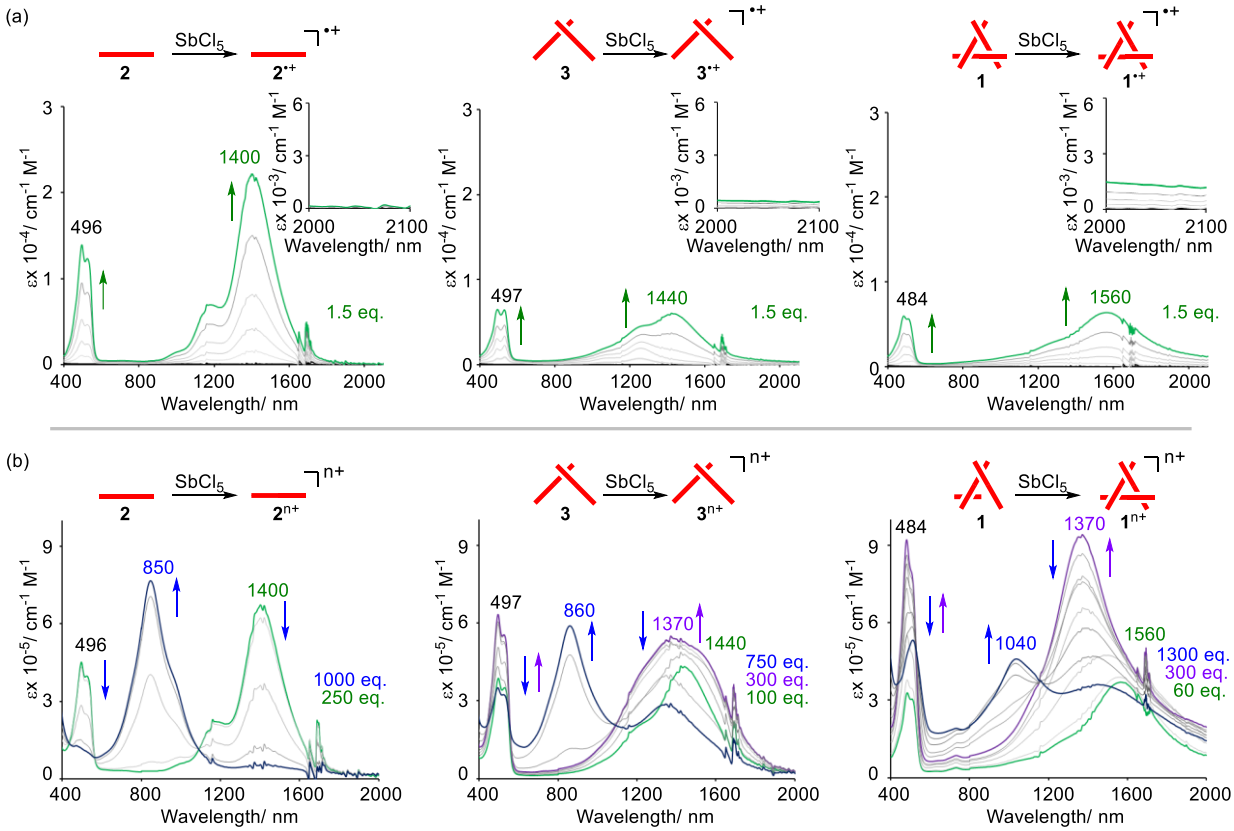

Figure 7 UV-vis-NIR absorption spectra in titration experiments for chemical oxidation of **2**, **3**, and **1** [(a) 100 μM and (b) 10 μM in CH_2Cl_2 at the start of titration] with $SbCl_5$ under N_2.

The interchain electron transfer in macrocycle $\mathbf{1}^{\cdot+}$ was suggested from the absorption spectroscopy experiments. ESR experiments were conducted using $\mathbf{2}^{\cdot+}$, $\mathbf{3}^{\cdot+}$, and $\mathbf{1}^{\cdot+}$ to further study the electron delocalization. The radical cation species were generated by the addition of 1.5 equivalents of $SbCl_5$. ESR spectra of $\mathbf{2}^{\cdot+}$, $\mathbf{3}^{\cdot+}$, and $\mathbf{1}^{\cdot+}$ at 293 K are shown in Figure 8. The spectra of them showed broad and structureless ESR signals resulting from a number of hydrogen nuclei with various hyperfine coupling constants, and it was difficult to obtain information on the spin delocalization from the hyperfine coupling patterns and ESR simulations. However, it is known that the peak-to-peak line width (ΔH) can be a measure of the spin delocalization in a molecule composed of multiple redox-active units based on equation 1.[15]

$$\Delta H_N = 1/\sqrt{N}\ \ \Delta H_M \qquad (1)$$

Here, ΔH_M is the linewidth of a monomer radical and ΔH_N is the linewidth when an unpaired spin is fully delocalized over N molecules (units) of the monomer. The observed line width of $\mathbf{2}^{\cdot+}$, $\mathbf{3}^{\cdot+}$,

and $\mathbf{1}^{\cdot+}$ were 4.13, 3.15, and 2.50 G, respectively, which were decreased by increasing the number of the bifluorenyl units. The ratios of ΔH to that of $\mathbf{2}^{\cdot+}$ were 0.76 and 0.61 for $\mathbf{3}^{\cdot+}$ and $\mathbf{1}^{\cdot+}$, respectively, and these values were close to $1/\sqrt{2} = 0.71$ and $1/\sqrt{3} = 0.58$. According to the equation 1, the radical spins in $\mathbf{3}^{\cdot+}$ and $\mathbf{1}^{\cdot+}$ were predicted to be delocalized over 1.72 and 2.73 bifluorenyl units, respectively. These results clearly show the delocalization of a spin in the whole molecule in not only $\mathbf{3}^{\cdot+}$ but also macrocycle $\mathbf{1}^{\cdot+}$ via fast hole hopping.

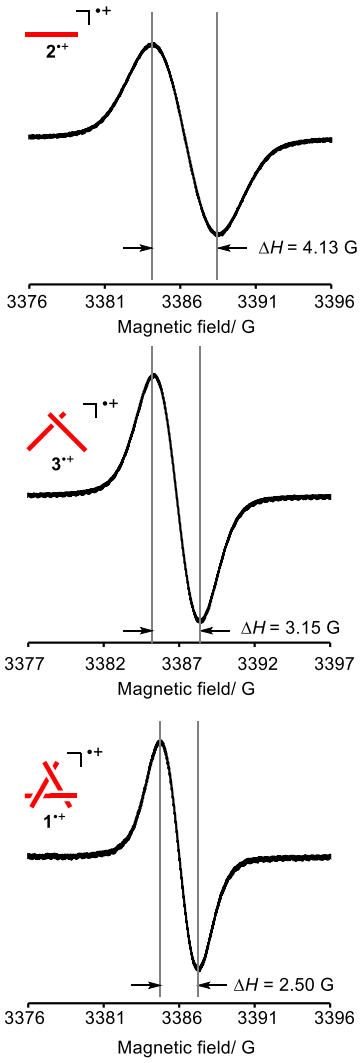

Figure 8 ESR spectra of $\mathbf{2}^{\cdot+}$, $\mathbf{3}^{\cdot+}$, and $\mathbf{1}^{\cdot+}$ at 293 K, where the radical cation species were generated in CH_2Cl_2 with 1.5 equivalents of $SbCl_5$ (Concentration of substrate: 0.5 mM for **2**, **3**, and **1**, respectively).

Conclusions

In conclusion, we designed and synthesized a cyclic [3]spirobifluorenylene compound **1** composed of three redox-active bifluorenyl units with bulky alkyl groups at the ends connected by

spirocarbons. By using the radical cationic states of **1** and its partial structures **2** and **3**, we investigated the electron transfer phenomena in π-conjugated systems including orthogonal π-conjugated chains. Small splitting (0.10 eV estimated by DFT calculation) of HOMOs of each bifluorenyl unit connected by spiro-conjugation allows the facile electron transfer between the orthogonal π-planes in **1**. The characterization of the macrocyclic compound **1** was carried out with absorption and fluorescence measurements and electrochemical analysis. Stepwise three one-electron oxidation processes were clearly observed for **1**, which is due to the Coulombic repulsion. DFT calculations of the radical cation species revealed a small HOMO–SOMO gap in $\mathbf{1}^{\cdot+}$, and the geometry-featured characteristic electron transition was visualized by NTO calculations. The radical cation species $\mathbf{1}^{\cdot+}$ generated by chemical oxidation showed a broadened and low-energy NIR absorption band exceeded over 2000 nm, assigned by the IVCT band. The results of the TD-DFT calculations and the absorption measurements confirmed the existence of the intramolecular electron transfer through spiro-conjugation in $\mathbf{1}^{\cdot+}$. Almost complete delocalization of a spin via hole hopping for the radical cation species $\mathbf{3}^{\cdot+}$ and $\mathbf{1}^{\cdot+}$ in the whole molecule is revealed by ESR experiments. We believe that this study gives a deeper insight into the intramolecular electron transfer and a new design concept of electronic materials including spiro-cyclic π-conjugated systems.

Conflicts of interest

There are no conflicts to declare.

Acknowledgements

We thank "Advanced Research Infrastructure for Materials and Nanotechnology in Japan (ARIM)" of the Ministry of Education, Culture, Sports, Science and Technology (MEXT) for the measurement of MALDI-TOF-MS analysis and CD spectra. We also thank Dr. Torii for the measurements of MALDI-TOF-MS analysis, Professors Eiji Yashima, Tomoyuki Ikai, and Kosuke Oki in Graduate School of Engineering, Nagoya University for the measurements of CD spectra, and Professors Hidehiko Nakagawa and Naoya Ieda in Graduate School of Pharmaceutical Sciences, Nagoya City University for the measurements of ESR spectra. We acknowledge the generous assistance of the Research Equipment Sharing Center at Nagoya City University. The computation was performed using Research Center for Computational Science, Okazaki, Japan (Project: 21-IMS-C190 and 22-IMS-C174). This work was supported by JSPS KAKENHI (20H02724), Nagase Science Technology Foundation, Tokyo Ohka Foundation for the Promotion of Science and Technology, Kumagai Foundation for Science and Technology, ENEOS Tonen General Research Grants, and Iketani Science and Technology Foundation. The synchrotron radiation experiment was performed at SPring-8 with the approval of the Japan Synchrotron Radiation Research Institute (JASRI) (Proposal No. 2022A1349).

References

1 (a) A. G. MacDiarmid, *Angew. Chem. Int. Ed. Engl.*, 2001, **40**, 2581–2590; (b) R. L. Carroll and C. B. Gorman, *Angew Chem Int Ed Engl.*, 2002, **41**, 4378–4400; (c) A. Facchetti, *Chem. Mater.*, 2011, **23**, 733–758; (d) J. Roncali, P. Leriche and P. Blanchard, *Adv. Mater.*, 2014, **26**, 3821–3838; (e) M. V. Ivanov, S. A. Reid and R. Rathore, *J. Phys. Chem. Lett.*, 2018, **9**, 3978–3986; (f) J. Urieta-Mora, I. García-Benito, A. Molina-Ontoria and N. Martín, *Chem. Soc. Rev.*, 2018, **47**, 8541–8571.

2 (a) J.-P. Launay, *Chem. Soc. Rev.*, 2001, **30**, 386–397; (b) K. D. Demadis, C. M. Hartshorn and T. J. Meyer, *Chem. Rev.*, 2001, **101**, 2655–2685; (c) B. S. Brunschwig, C. Creutz and N. Sutin, *Chem. Soc. Rev.*, 2002, **31**, 168–184; (d) J. Hankache and O. S. Wenger, *Chem. Rev.*, 2011, **111**, 5138–5178; (e) A. Heckmann and C. Lambert, *Angew. Chem. Int. Ed. Engl.*, 2012, **51**, 326–392.

3 (a) T. S. Navale, K. Thakur, V. S. Vyas, S. H. Wadumethrige, R. Shukla, S. V. Lindeman and R. Rathore, *Langmuir*, 2012, **28**, 71–83; (b) H. Qi, J. Chang, S. H. Abdelwahed, K. Thakur, R. Rathore and A. J. Bard, *J. Am. Chem. Soc.*, 2012, **134**, 16265–16274; (c) J.-R. Mistry, S. Montanaro and I. A. Wright, *Mater. Adv.*, 2023, **4**, 787–803.

4 (a) H. E. Simmons and T. Fukunaga, *J. Am. Chem. Soc.*, 1967, **89**, 5208–5215; (b) R. Hoffmann, A. Imamura and G. D. Zeiss, *J. Am. Chem. Soc.*, 1967, **89**, 5215–5220; (c) H. Dürr and R. Gleiter, *Angew. Chem. Int. Ed. Engl.*, 1978, **17**, 559–569; (d) R. Gleiter and G. Haberhauer, Aromaticity and Other Conjugation Effects, Wiley-VCH, Wiinheim, 2012, 166.

5 (a) T. P. I. Saragi, T. Spehr, A. Siebert, T. Fuhrmann-Lieker and J. Salbeck, *Chem. Rev.*, 2007, **107**, 1011–1065; (b) C. Poriel, L. Sicard and J. Rault-Berthelot, *Chem. Commun.*, 2019, **55**, 14238–14254; (c) S. Liu, D. Xia and M. Baumgarten, *ChemPlusChem*, 2021, **86**, 36–48; (d) Y. Wei, Y. Yan, X. Li, L. Xie and W. Huang, *Org. Biomol. Chem.*, 2022, **20**, 73–97.

6 (a) A. Schweig, U. Weidner, D. Hellwinkel and W. Krapp, *Angew. Chem. Int. Ed. Engl.*, 1973, **12**, 310–311; (b) B. H. Boo, Y. S. Choi, T.-S. Kim, S. K. Kang, Y. H. Kang and S. Y. Lee, *J. Mol. Struct.*, 1996, **377**, 129–136.

7 Z. Hawash, L. K. Ono and Y. B. Qi, *Adv. Mater. Interfaces*, 2018, **5**, 1700623.

8 Theoretical study: A. Farazdel, M. Dupuis, E. Clementi and A. Aviram, *J. Am. Chem. Soc.*, 1990, **112**, 4206–4214.

9 Experimental study: (a) P. Maslak, M. P. Augustine and J. D. Burkey, *J. Am. Chem. Soc.*, 1990, **112**, 5359–5360; (b) Y. Hirao, M. Urabe, A. Ito and K. Tanaka, *Angew. Chem. Int. Ed. Engl.*, 2007, **46**, 3300–3303; (c) A. Ito, K. Hata, K. Kawamoto, Y. Hirao, K. Tanaka, M. Shiro, K. Furukawa and T. Kato, *Chem. Eur. J.*, 2010, **16**, 10866–10878; (d) F. Barrière, C. Poriel and J. Rault-Berthelot, *Electrochim. Acta*, 2013, **110**, 735–740; (e) Q. Yan, Y. Guo, A.

Ichimura, H. Tsuji and E. Nakamura, *J. Am. Chem. Soc.*, 2016, **138**, 10897–10904; (f) H. C. Schmidt, C. B. Larsen and O. S. Wenger, *Angew. Chem. Int. Ed. Engl.*, 2018, **57**, 6696–6700; (g) H. Hamada, Y. Itabashi, R. Shang and E. Nakamura, *J. Am. Chem. Soc.*, 2020, **142**, 2059–2067; (h) X. Zhao, J. P. O'Connor, J. D. Schultz, Y. J. Bae, C. Lin, R. M. Young and M. R. Wasielewski, *J. Phys. Chem. B*, 2021, **125**, 6945–6954; (i) E. Sebastian and M. Hariharan, *J. Am. Chem. Soc.*, 2021, **143**, 13769–13781.

10 M. V. Ivanov, S. H. Wadumethrige, D. Wang and R. Rathore, *Chem. Eur. J.*, 2017, **23**, 8834–8838.

11 (a) J. Oniki, T. Moriuchi, K. Kamochi, M. Tobisu and T. Amaya, *J. Am. Chem. Soc.*, 2019, **141**, 18238–18245; (b) K. Zhu, K. Kamochi, K. Kamochi, T. Kodama, M. Tobisu and T. Amaya, *Chem. Sci.*, 2020, **11**, 9604–9610. c) K. Nakagawa, K. Akimoto, B. Nakayasu, S. Nagashima, M. Tobisu, M. P. Schramm, S. Aoyagi, T. Amaya, *Org. Lett.*, in press (doi: 10.1021/acs.orglett.3c02074).

12 W. Huang, T. L. E. Henderson, A. M. Bond and K. B. Oldham, *Anal. Chim. Acta*, 1995, **304**, 1–15.

13 a) M. Renz, K. Theilacker, C. Lambert and M. Kaupp, *J. Am. Chem. Soc.*, 2009, **131**, 16292–16302; b) M. Parthey and M. Kaupp, *Chem. Soc. Rev.*, 2014, **43**, 5067– 5088.

14 N. G. Connelly and W. E. Geiger, *Chem. Rev.*, 1996, **96**, 877–910.

15 J. R. Norris, R. A. Uphaus, H. L. Crespi and J. J. Katz, *Proc. Nat. Acad. Sci.*, 1971, **68**, 625–628.